Kybernetika

Özhan Bingöl; Haci Mehmet Güzey

Design of a neuro-sliding mode controller for interconnected quadrotor UAVs carrying a suspended payload

Kybernetika, Vol. 59 (2023), No. 5, 670–699

Persistent URL: http://dml.cz/dmlcz/151982

KYBERNETIKA — VOLUME *59* (2023), NUMBER 5, PAGES 670–699

DESIGN OF A NEURO-SLIDING MODE CONTROLLER FOR INTERCONNECTED QUADROTOR UAVS CARRYING A SUSPENDED PAYLOAD

Özhan Bingöl and Haci Mehmet Güzey

In this study, a generalized system model is derived for interconnected quadrotor UAVs carrying a suspended payload. Moreover, a novel neural network-based sliding mode controller (NSMC) for the system is suggested. While the proposed controller uses the advantages of the robust structure of sliding mode controller (SMC) for the nonlinear system, the neural network component eliminates the chattering effects in the control signals of the SMC and increases the efficiency of the SMC against time-varying dynamic uncertainties. After the controller design is carried out, a comprehensive stability analysis based on Lyapunov theory is given to assure the asymptotic stability of the system. Finally, extensive numerical simulations with detailed comparisons are used to verify the effectiveness of the proposed controller.

Keywords: autonomous UAV, interconnected system, neuro-sliding mode control, payload transportation

Classification: 93D05, 93D21, 68T40

1. INTRODUCTION

The number of studies on quadrotor UAVs has recently increased significantly [4, 17, 19, 30, 45, 48]. Due to their advantages over conventional aircraft, including smaller construction, agility, low prices, and maneuverability, quadrotors stand out as the most popular UAVs in both civil and military applications [18, 34]. As a result of their widespread use, studies on UAVs and load-carrying applications are rapidly increasing. The quadrotor is a highly suitable candidate for autonomous transportation due to its high manoeuvrability, vertical take-off and landing capability, and the ability to transport loads of almost its own body weight [12]. Despite their superior advantages, their limited load capacities severely restrict their load-carrying applications. In addition, in the event of any malfunction, it is possible to lose the load along with the quadrotor [41]. Therefore, using multiple quadrotors significantly increases load capacity and also increases the safety of the cargo in the event of any malfunction.

Due to their under-actuated structure, the control problem of a quadrotor itself presents many difficulties. In addition to these difficulties, carrying a suspended payload entirely alters the flight dynamics of the quadrotor, posing new challenges in the vehicle's

DOI: 10.14736/kyb-2023-5-0670

control scheme that must be overcome [5]. The performance of the control algorithms developed for their control, as well as the structural elements of the quadrotors, are critical to a successful flight. [28].

Much research in the literature has investigated the difficulty of controlling quadrotor UAVs [6, 16, 20, 23, 47]. There are also many studies conducted on systems carrying payloads with one or two UAVs [3, 8, 14, 31, 32, 36, 38, 46]. But there is a limited amount of research on load-transporting systems with more than two quadrotors. In [21], a comprehensive study of the inverse kinematics problem for payloads transported by three quadrotors is explored. An inverse kinematics problem is formulated based on the static equilibrium equations, and an efficient analytical algorithm based on dialytic elimination is presented to solve the inverse kinematics problem. However, the number of quadrotors used in the study is limited to three. To extend the number of quadrotor UAVs in [15], a payload-leading control for multiple quadrotor system was considered. The desired rotorcraft states were derived by kinematics analysis with knowledge of payload states and desired cable forces. As a controller, a PID-based control structure was given. The proposed controller in Shirani et al. [37] was also developed for any number of quadrotors. An LQR-PID controller was suggested to guarantee a fixed formation for UAVs to successfully transport the payload. With a similar approach, Dhiman et al. [9] suggested a cooperative control structure that was designed to control the movement of the quadrotors and the suspended load for n-number of quadrotors with a UAV formation that ensures the load distribution among UAVs. A combination of PID and PD controllers was used as the controller. In a different approach compared to traditional controllers, Li et al. [27] used a vision-based controller design for three quadrotors that transported fixed-shaped cargo. A distributed estimation approach was used, allowing each quadrotor to independently estimate cable direction and speed.

Choosing the right controller for nonlinear systems is crucial. Sliding mode control (SMC), which is a robust control technique against system uncertainties, parameter changes, and external disturbances, stands out as a frequently preferred technique in the control of nonlinear systems [39]. Zhou et al. [49] compared a PD controller with a sliding mode controller to control a quadrotor that was carrying a suspended payload and demonstrated the robustness of the sliding mode controller against load swings and uncertainties. In [40], an adaptive frictional sliding mode controller for a quadrotor transporting a varying payload was developed, and numerical simulations showed the success of sliding mode-based controllers. Other recent work has also demonstrated the effectiveness of SMC-based controllers in the applications of load transportation with quadrotor UAVs [29, 44]. Even though SMC provides robust control for nonlinear systems, in the case of time-varying dynamic uncertainties, a full knowledge of the plant dynamics is needed to calculate a proper controller [11, 24]. Many different methods have been developed in the literature to successfully eliminate this phenomenon [25, 33, 22, 42]. With the recent developments in the area of artificial intelligence, artificial intelligence-based controllers have started to be developed for different nonlinear systems in order to eliminate the computational burden of SMC [7, 13]. A neural network controller with a learning rule based on a sliding mode algorithm can be utilized to ensure the computation of an unknown component of the equivalent control when there are uncertainties regarding the plant. In addition to that, this controller has the quality

of being robust in the face of parameter changes and external disruptions. In our previous work [2], a novel neuro-sliding mode controller was suggested for a quadrotor that carries a suspended payload. As an extension to that study, a similar controller structure was developed for an interconnected quadrotor UAV system carrying a suspended payload. The key contributions of this work are listed below:

1) In this work, a generalized structure for interconnected quadrotor UAVs system is presented. A detailed nonlinear model of the system is derived. The system is modeled in such a way that the payload can be transported using any number of UAVs. In the suspended payload transportation scenario, it is assumed that one of the UAVs initially has the desired trajectory. The rest of the UAV's desired trajectories are calculated through our geometric approach. To do so, the desired angles of each quadrotor are derived first. Then, the desired x and y positions of the payload and each UAV are calculated. Once the carrying angles and desired trajectories are obtained, interconnected forces are derived the forces acting on the payload.

2) Furthermore, a novel neuro-sliding mode controller is proposed. With the help of the neural network component, the controller can successfully control the system without knowing the quadrotor dynamics and can update the system dynamics against uncertainties that change over time with the updated learning structure. The incorporation of a neural network component into the control framework minimizes control input value and chattering while improving error performance.

3) To ensure the closed-loop stability of the multi-quadrotor load transportation system, a comprehensive study of the system's stability is offered.

In order to show the efficiency of the proposed controller, the designed system was first controlled with an SMC, assuming the dynamics are known. Then it was controlled with an updated SMC, assuming the dynamics were unknown. Finally, the system was controlled with the proposed controller, and simulation results were compared.

The article is structured as follows: Information on quadrotor dynamics, neural networks, and interconnected quadrotor UAVs system dynamics, respectively, is given in Section 2. The control structures proposed in the study are developed in section 3. In order to show the effectiveness of the developed controller, simulations are made in section 4. Conclusions are given in section 5.

Next, a short background and problem formulation is given.

2. BACKGROUND AND PROBLEM FORMULATION

This chapter begins with a basic overview of quadrotor dynamics and neural networks. Then, a problem formulation on the interconnected dynamics of UAVs carrying payloads is presented, as is the derivation of desired trajectories for each UAV.

2.1. Quadrotor dynamics

In order for the quadrotor to move along the desired trajectory, symmetrically placed rotors are used. For this purpose, four input signals have been designated. The vertical

motion of the quadrotor in the z-axis is controlled by the u_1 input. It provides upward or downward movement by boosting or reducing the speeds of all propellers at the same rate. The u_2 input generates torque along the x-axis by increasing or decreasing the speed of the left propeller while also increasing or decreasing the speed of the right propeller by the same amount. Thus, the roll motion is acquired along the x-axis. The pitch motion is obtained by u_3 input. The u_3 input changes the speed of the rear and front propellers, causing motion in the y-axis. The yaw motion along the z-axis is obtained with u_4 input by reducing or boosting the speeds of the left and right propellers simultaneously, while boosting or reducing the speeds of the rear and front propellers.

Since the rotors are assumed to be positioned symmetrically, as shown in Figure 1, aerodynamic torques and gyroscopic effects are assumed to cancel each other out in flight. To denote the position and attitude of a quadrotor, two reference frames are specified. The earth frame states the position of the UAV's center of gravity, given by $E\{x, y, z\}$, and the body fixed frame, denoted by $B\{x, y, z\}$.

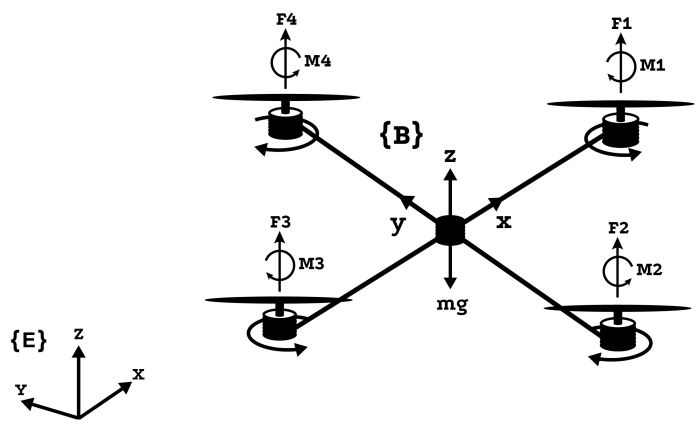

Fig. 1. Model of quadrotor.

Using Lagrange equations dynamical model of quadrotor could be obtained as [1]:

$$\begin{aligned}
\ddot{x} &= \frac{1}{m}\left(\cos\phi\sin\theta\cos\psi + \sin\phi\sin\psi\right)u_1 - \frac{K_1\dot{x}}{m} \\
\ddot{y} &= \frac{1}{m}\left(\cos\phi\sin\theta\sin\psi + \sin\phi\cos\psi\right)u_1 - \frac{K_2\dot{y}}{m} \\
\ddot{z} &= \frac{1}{m}\left(\cos\phi\cos\theta\right)u_1 - g - \frac{K_3\dot{z}}{m} \\
\ddot{\phi} &= \dot{\theta}\dot{\psi}\frac{I_y - I_z}{I_x} + \frac{J_r}{I_x}\Omega_r\dot{\theta} + \frac{l}{I_x}u_2 - \frac{K_4 l}{I_x}\dot{\phi} \\
\ddot{\theta} &= \dot{\psi}\dot{\phi}\frac{I_z - I_x}{I_y} + \frac{J_r}{I_y}\Omega_r\dot{\phi} + \frac{l}{I_y}u_3 - \frac{K_5 l}{I_y}\dot{\theta}
\end{aligned} \tag{1}$$

$$\ddot{\psi} = \dot{\phi}\dot{\theta}\frac{I_x - I_y}{I_z} + \frac{1}{I_z}u_4 - \frac{K_6}{I_z}\dot{\psi}$$

where (ϕ, θ, ψ) are roll, pitch and yaw angles respectively; (x, y, z) are representing UAV's positions in three axes; m is the mass of quadrotor; g is acceleration of gravity; l is the distance to the propellers from the center of the quadrotor; I_x, I_y, I_z are the inertia with respect to each axes; J_r is the inertia of the propeller; K_i (i =1, 2, , 6) are the drag coefficients, and u_i (i = 1, 2, 3, 4) are the virtual inputs defined as:

$$\begin{aligned} u_1 &= (F_1 + F_2 + F_3 + F_4) \\ u_2 &= (-F_2 + F_4) \\ u_3 &= (-F_1 + F_3) \\ u_4 &= \frac{d\,(-F_1 + F_2 - F_3 + F_4)}{b} \end{aligned} \tag{2}$$

where rotor thrusts are represented as $F_i(i = 1, 2, 3, 4), b$ is the lift coefficient, d is the force-to-moment scaling vector.

2.2. Neural network

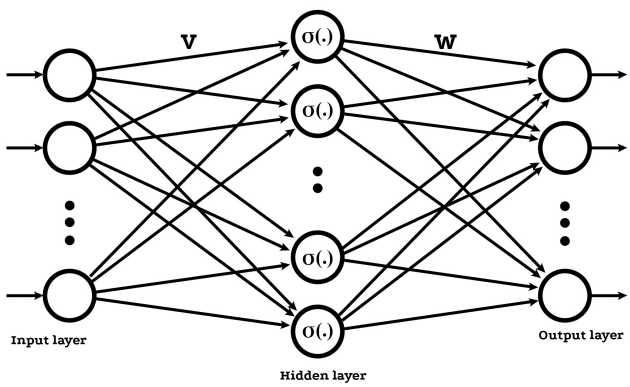

Fig. 2. Neural network structure.

In this work, a two-layer neural network (NN) structure as shown in Figure 2 is used to estimate uncertain dynamics. The neural network component learns the system dynamics. Thus, it reduces the control input amplitude significantly while eliminating the chattering effect. The first layer is hidden layer that contains adjustable hidden weights, $W \in \mathbb{R}^{(Nh \times ko)}$, and the second layer consists of randomly determined constants, $\bar{N} \in \mathbb{R}^{(ki \times Nh)}$ where ki is input count and ko is output count. Nh represents the number of neurons in the hidden layer. Estimation function, $f(x)$, can be given as $f(x) = W^T\sigma\left(\bar{N}^T x\right) + \varepsilon$ where ε is the bounded NN estimation error that satisfies

$\|\varepsilon\| < \varepsilon_M$, and $\sigma(\bullet) : \mathbb{R}^a \to \mathbb{R}^L$ is the activation function for the hidden layer. Because the input-layer weights $\bar{N} \in \mathbb{R}^{ki \times Nh}$ are randomly chosen, for any input x, the estimation is viable; hence the activation function,$\sigma(x) = \sigma\left(\bar{N}^T x\right)$, establishes a stochastic base in the compact set S [26]. As an activation function a tangent hyperbolic function is chosen in this study. It is also assumed that target weights are limited to a known positive value W_M satisfying $\|W\|_F < W_M$ on any compact subset of $\mathbb{R}^n$ [10]. Moreover, $\|\bullet\|$ and $\|\bullet\|_F$ are considered as the vector and Frobenius norm respectively [26].

Definition 2.1. (semi-globally uniformly ultimately bounded (SGUUB)) Any equilibrium point x_e is said to be SGUUB if there is an area around the origin with a radius r where $S(0, r) = S_r \subset \mathbb{R}^n$ so that for all $x_0 \in \mathbb{R}^n$, there exists a bound $B > 0$ and a time $T(B, x_0)$ such that $\|x(t) - x_e\| \leq B$ for all $t > t_0 + T$.

2.3. Formulation of desired trajectories

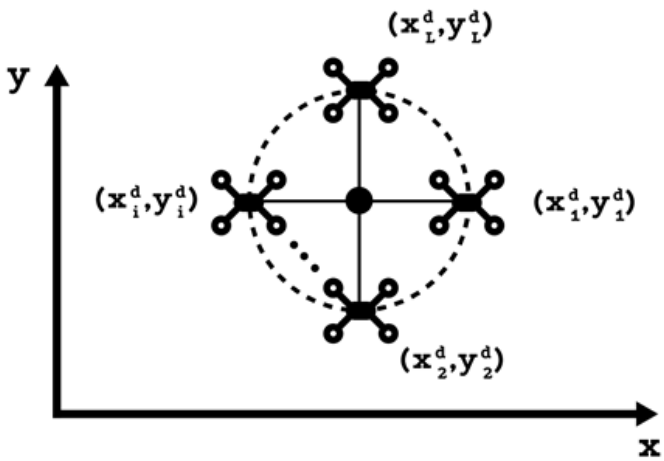

Fig. 3. Circular formation of quadrotors carrying a payload.

This study develops a model of interconnected quadrotor UAVs for transporting a suspended payload. For this objective, a circular configuration, as illustrated in Figure 3, is designed for an N number of quadrotor UAVs with equal z-positions. The payload is in the middle, and the quadrotors' angles with regard to each other are equal. The trajectory of one quadrotor is assumed to be known, and the remaining quadrotors can compute their trajectories using the geometric technique provided below, using the desired trajectory of the first quadrotor as a reference.

To calculate trajectories, the position of the first quadrotor identified with x_L^d, y_L^d in $x - y$ plain is assumed to be known. Let the distance of each quadrotor to payload in $x - y$ plain be L_{xy} since it will be depending on the cable length L. Desired L_{xy} can be given as:

$$L_{xy} = L\sin(\alpha^d) \tag{3}$$

where α^d is desired α angle in $x - z$ plain, as shown in Figure 4, given as:

$$\alpha^d = \arccos\left(|\frac{z_L - z_P}{L}|\right) \tag{4}$$

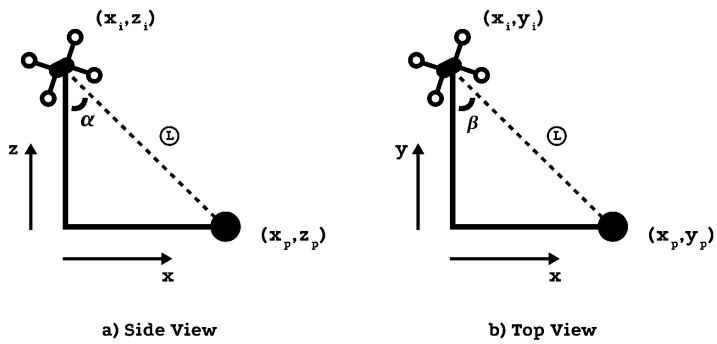

Fig. 4. α and β angles respectively.

where z_L is leader quadrotor's z position and z_P is z position of payload. The ${\alpha_L}^d$ and ${\beta_L}^d$ angles of leader quadrotor are known in order to establish a circular formation. ${\beta_i}^d$ is desired angle of ith quadrotor in $x - y$ plain and as it is shown in Figure 4 and it can be calculated for each quadrotor as:

$$\beta_i^d = \beta_L^d + \frac{360(i-1)}{N} \quad \forall i = 2, 3, \ldots, N. \tag{5}$$

Then to find the position of each quadrotor in $x - y$ plain first the position of payload can be calculated by using leader quadrotor position as:

$$\begin{aligned} x_P^d &= x_L^d + L_{xy}\cos(\beta_L^d) \\ y_P^d &= y_L^d + L_{xy}\sin(\beta_L^d) \end{aligned} \tag{6}$$

where x_P^d and y_P^d are desired x and y positions of payload. After calculating the position of payload, x_i^d and y_i^d coordinates for ith quadrotor in $x - y$ plain can be generalized as:

$$\begin{aligned} x_i^d &= x_p^d + L_{xy}\cos(\beta_i^d) \\ y_i^d &= y_p^d + L_{xy}\sin(\beta_i^d). \end{aligned} \tag{7}$$

2.4. Formulation of interconnected dynamics

Once the trajectories of each quadrotor are calculated, the forces acting on each one can be obtained and the total dynamics of the system can be deduced. To obtain forces, the payload is modelled as a three-dimensional point pendulum mass, as shown in Figure 5. Moreover, following presumptions formed the basis of the payload model:

1) Payloads can only tilt in two directions since the payload is not allowed to spin around the cable axis.
2) A stiff, weightless, nonelastic cable is used to sustain the load.
3) As the center of mass of the quadrotor is located at the cable joint, the tensile stress of the cable does not effect the rotation of the quadrotor.

Using angles in equations (4) and (5) we can define forces acting on each axis on each quadrotor as:

$$\begin{aligned} F_{xi} &= \sum_{j=1, j\neq i}^{N} U_{2j} \cos(\beta_j(t)) \\ F_{yi} &= \sum_{j=1, j\neq i}^{N} U_{3j} \sin(\beta_j(t)) \\ F_{zi} &= \left(\sum_{j=1, j\neq i}^{N} [U_{1j} \sin(\alpha_j(t))] \right) - m_L g \end{aligned} \tag{8}$$

where, U_{1j}, U_{2j}, U_{3j} are control inputs of the jth UAV on x, y and z directions, respectively, m_L is payload mass, g is gravity force and F_{xi}, F_{yi}, F_{zi} are total forces acting on each quadrotor on corresponding axis. Combining these interconnection forces with quadrotor dynamics in equation (1) the dynamical equation of the ith quadrotor can be given as:

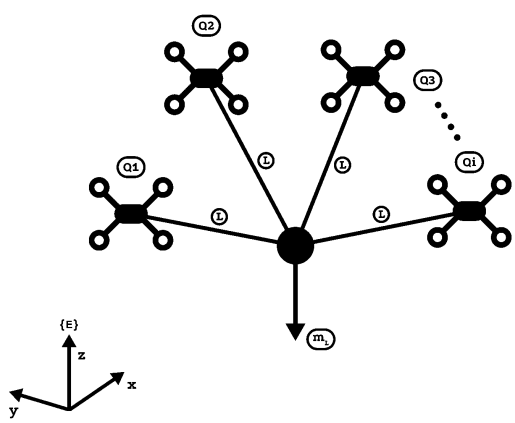

Fig. 5. The interconnected system.

$$
\begin{aligned}
m\ddot{x}_i &= (\cos\phi_i \sin\theta_i \cos\psi_i + \sin\phi_i \sin\psi_i)\, u_{1i} - K_1\dot{x}_i - F_{xi} \\
m\ddot{y}_i &= (\cos\phi_i \sin\theta_i \sin\psi_i + \sin\phi_i \cos\psi_i)\, u_{1i} - K_2\dot{y}_i - \ F_{yi} \\
m\ddot{z}_i &= (\cos\phi_i \cos\theta_i)\, u_{1i} - mg - K_3\dot{z}_i + F_{zi} \\
\ddot{\phi}_i &= \dot{\theta}_i\dot{\psi}_i \frac{I_y - I_z}{I_x} + \frac{J_r}{I_x}\Omega_{ri}\dot{\theta}_i + \frac{l}{I_x}u_{2i} - \frac{K_4 l}{I_x}\dot{\phi}_i \\
\ddot{\theta}_i &= \dot{\psi}_i\dot{\phi}_i \frac{I_z - I_x}{I_y} + \frac{J_r}{I_y}\Omega_{ri}\dot{\phi}_i + \frac{l}{I_y}u_{3i} - \frac{K_5 l}{I_y}\dot{\theta}_i \\
\ddot{\psi}_i &= \dot{\phi}_i\dot{\theta}_i \frac{I_x - I_y}{I_z} + \frac{1}{I_z}u_{4i} - \frac{K_6}{I_z}\dot{\psi}_i.
\end{aligned}
\tag{9}
$$

Note that the interconnected dynamics affect only the position dynamics of quadrotors since the cables are attached to the quadrotors' mass centers. Therefore, interconnections do not have any effect on the dynamics of quadrotors' angular dynamics.

Next controller designs are given.

3. CONTROLLER DESIGN

In this section, the proposed controller is designed. The controller is developed in three steps. First, an SMC is developed with the assumption that the dynamics are known. Next, an SMC with unknown dynamics is derived, and finally, the proposed controller is given in the presence of uncertain dynamics. The uncertain dynamics are learned through neural network components so that both the chattering effect is reduced and the system is successfully controlled without fully knowing the dynamics of the controlled system. Moreover, with the updated learning structure, it can update system dynamics successfully even if there are uncertainties that change over time. The proposed neuro-sliding mode control structure is given in Figure 6.

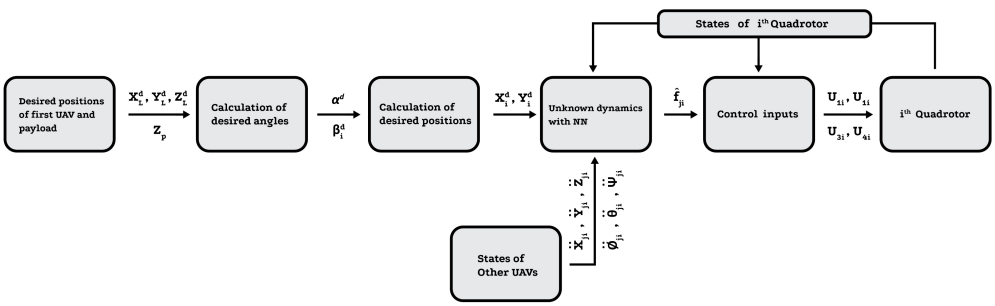

Fig. 6. Overall structure of the system.

3.1. Sliding mode controller design with known dynamics

In the first stage of the controller design, a classical SMC design will be realized by making the assumption that the dynamics of all of the quadrotors in the system as well as the dynamics added by the payload on the quadrotors are fully known. This will allow a comparison of how chattering effects occur in control signals and how unknown dynamics affect reference tracking when the effect of unknown dynamics is considered in a classical SMC design. It can also be easily observed that even assuming the dynamics are known, the magnitudes of the control signals will be unacceptably high. In order to perform the controller design more conveniently dynamics in equation (9) are transformed to the following form [43];

$$\begin{cases} \ddot{z}_i = f_{1i} + \ g_{1i}u_{1i} \\ \begin{cases} \ddot{x}_i = f_{2i} + \ g_{2i}u_{2i} \\ \ddot{\phi}_i = f_{3i} + g_{3i}u_{2i} \end{cases} \\ \begin{cases} \ddot{y}_i = f_{4i} + g_{4i}u_{3i} \\ \ddot{\theta}_i = f_{5i} + \ g_{5i}u_{3i} \end{cases} \\ \ddot{\psi}_i = f_{6i} + g_{6i}u_{4i} \end{cases} \tag{10}$$

where

$$\begin{aligned} f_{1i} &= -g - \frac{K_3\dot{z}_i}{m} + \frac{F_{zi}}{m}, g_{1i} = \frac{\cos\phi_i \cos\theta_i}{m} \\ f_{2i} &= \frac{(\cos\phi_i \sin\theta_i \cos\psi_i + \sin\phi_i \sin\psi_i)\, u_{1i}}{m} - \frac{K_1\dot{x}_i}{m}, g_{2i} = 0 \\ f_{3i} &= \frac{\left(\dot{\theta}_i\dot{\psi}_i\,(I_y - I_z) + J_r\dot{\theta}_i\Omega_{ri} - K_4 l\dot{\phi}_i\right)}{I_x}, g_{3i} = \frac{l}{I_x} \\ f_{4i} &= \frac{(\cos\phi_i \sin\theta_i \sin\psi_i + \sin\phi_i \cos\psi_i)\, u_{1i}}{m} - \frac{K_2\dot{y}_i}{m}, g_{4i} = 0 \\ f_{5i} &= \frac{\left(\dot{\psi}_i\dot{\phi}_i\,(I_z - I_x) + J_r\dot{\phi}_i\Omega_{ri} - K_5 l\dot{\theta}_i\right)}{I_y}, g_{5i} = \frac{l}{I_y} \\ f_{6i} &= \frac{\left(\dot{\phi}_i\dot{\theta}_i\,(I_x - I_y) - K_6\dot{\psi}_i\right)}{I_z}, g_{6i} = \frac{1}{I_z}. \end{aligned} \tag{11}$$

The sliding surface functions can be generalized as:

$$s_k = a_{k1}\left(\dot{q}_{k1d} - \dot{q}_{k1}\right) + a_{k2}\left(q_{k1d} - q_{k1}\right) + a_{k3}\left(\dot{q}_{k2d} - \dot{q}_{k2}\right) + a_{k4}\left(q_{k2d} - q_{k2}\right) \tag{12}$$

where q_k is any arbitrary variant and q_{kd} is the desired value of q_k, the coefficients $a_{kj}(j, k = 1, 2, 3, 4)$ were acquired in our previous study [2] in detail. With the right coefficients, the sliding surface functions can be given as [43]:

$$
\begin{aligned}
s_{1i} &= a_{11}\left(\dot{z}_i^d - \dot{z}_i\right) + a_{12}\left(z_i^d - z_i\right) \\
s_{2i} &= a_{21}\left(\dot{x}_i^d - \dot{x}_i\right) + a_{22}\left(x_i^d - x_i\right) + a_{23}\left(\dot{\phi}_i^d - \dot{\phi}_i\right) + a_{24}\left(\phi_i^d - \phi_i\right) \\
s_{3i} &= a_{31}\left(\dot{y}_i^d - \dot{y}_i\right) + a_{32}\left(y_i^d - y_i\right) + a_{33}\left(\dot{\theta}_i^d - \dot{\theta}_i\right) + a_{34}\left(\theta_i^d - \theta_i\right) \\
s_{4i} &= a_{41}\left(\dot{\psi}_i^d - \dot{\psi}_i\right) + a_{42}\left(\psi_i^d - \psi_i\right)
\end{aligned} \tag{13}
$$

where, a_{11},a_{12},a_{41},$a_{42} > 0$, $a_{13} = a_{14} = a_{43} = a_{44} = 0$. By taking the derivatives of sliding manifolds and inserting the dynamics from equation (11) they yield as:

$$
\begin{aligned}
\dot{s}_{1i} &= a_{11}\left(\ddot{z}_i^d - f_{1i} + g_{1i}u_{1i}\right) + a_{12}\left(\dot{z}_i^d - \dot{z}_i\right) \\
\dot{s}_{2i} &= a_{21}\left(\ddot{x}_i^d - f_{2i} + g_{2i}u_{2i}\right) + a_{22}\left(\dot{x}_i^d - \dot{x}_i\right) \\
&\quad + a_{23}\left(\ddot{\phi}_i^d - f_{3i} + g_{3i}u_{2i}\right) + a_{24}\left(\dot{\phi}_i^d - \dot{\phi}_i\right) \\
\dot{s}_{3i} &= a_{31}\left(\ddot{y}_i^d - f_{4i} + g_{4i}u_{3i}\right) + a_{32}\left(\dot{y}_i^d - \dot{y}_i\right) \\
&\quad + a_{33}\left(\ddot{\theta}_i^d - f_{5i} + g_{5i}u_{3i}\right) + a_{34}\left(\dot{\theta}_i^d - \dot{\theta}_i\right) \\
\dot{s}_{4i} &= a_{41}\left(\ddot{\psi}_i^d - f_{6i} + g_{6i}u_{4i}\right) + a_{42}\left(\dot{\psi}_i^d - \dot{\psi}_i\right).
\end{aligned} \tag{14}
$$

To stabilize the sliding surfaces, following theorem is provided.

Theorem 3.1. (Sliding mode controller design with known dynamics) By taking the sliding surface functions in equation (14) let the controllers be:

$$
\begin{aligned}
u_{1i} &= \frac{1}{a_{11}g_{1i}}\left\{a_{11}\left(\ddot{z}_i^d - f_{1i}\right) + a_{12}\left(\dot{z}_i^d - \dot{z}_i\right) + \eta_{1i}s_{1i} \quad \right\} \\
u_{2i} &= \frac{1}{a_{21}g_{2i} + a_{23}g_{3i}}\left\{\begin{array}{l} a_{21}\left(\ddot{x}_i^d - f_{2i}\right) + a_{22}\left(\dot{x}_i^d - \dot{x}_i\right) \\ + a_{23}\left(\ddot{\phi}_i^d - f_{3i}\right) + a_{24}\left(\dot{\phi}_i^d - \dot{\phi}_i\right) + \eta_{2i}s_{2i} \end{array}\right\} \\
u_{3i} &= \frac{1}{a_{31}g_{4i} + a_{33}g_{5i}}\left\{\begin{array}{l} a_{31}\left(\ddot{y}_i^d - f_{4i}\right) + a_{32}\left(\dot{y}_i^d - \dot{y}_i\right) \\ + a_{33}\left(\ddot{\theta}_i^d - f_{5i}\right) + a_{34}\left(\dot{\theta}_i^d - \dot{\theta}_i\right) + \eta_{3i}s_{3i} \end{array}\right\} \\
u_{4i} &= \frac{1}{a_{41}g_{6i}}\left\{\left(\ddot{\psi}_i^d - f_{6i}\right) + a_{42}\left(\dot{\psi}_i^d - \dot{\psi}_i\right) + \eta_{4i}s_{4i}\right\}
\end{aligned} \tag{15}
$$

with i index of quadrotors and $\eta_{ki} > 0\ \forall k = 1, 2, 3, 4$ being constant parameters, all sliding surfaces are asymptotically stable.

P r o o f . Let the Lyapunov function for ith quadrotor be as:

$$
V_i = \sum_{k=1}^{4} \frac{s_{ki}^2}{2} \tag{16}
$$

and by taking the derivative of equation (16) :

$$\begin{aligned}\dot{V}_i &= \sum_{k=1}^{4} s_{ki}\dot{s}_{ki} \\ &= s_{1i}\left\{a_{11}\left(\ddot{z}_i^d - f_{1i} + g_{1i}u_{1i}\right) + a_{12}\left(\dot{z}_i^d - \dot{z}_i\right)\right\} \\ &+ s_{2i}\left\{\begin{array}{l} a_{21}\left(\ddot{x}_i^d - f_{2i} + g_{2i}u_{2i}\right) + a_{22}\left(\dot{x}_i^d - \dot{x}_i\right) \\ + a_{23}\left(\ddot{\phi}_i^d - f_{3i} + g_{3i}u_{2i}\right) + a_{24}\left(\dot{\phi}_i^d - \dot{\phi}_i\right)\end{array}\right\} \\ &+ s_{3i}\left\{\begin{array}{l} a_{31}\left(\ddot{y}_i^d - f_{4i} + g_{4i}u_{3i}\right) + a_{32}\left(\dot{y}_i^d - \dot{y}_i\right) \\ + a_{33}\left(\ddot{\theta}_i^d - f_{5i} + g_{5i}u_{3i}\right) + a_{34}\left(\dot{\theta}_i^d - \dot{\theta}_i\right)\end{array}\right\} \\ &+ s_{4i}\left\{a_{41}\left(\ddot{\psi}_i^d - f_6 + g_{6i}u_{4i}\right) + a_{42}\left(\dot{\psi}_i^d - \dot{\psi}_i\right)\right\}.\end{aligned} \tag{17}$$

Use the controller signals in equation (15) into equation (17) and obtain:

$$\dot{V}_i = \sum_{k=1}^{4} -\eta_{ki}s_{ki}^2. \tag{18}$$

Therefore, the system is asymptotically stable. This concludes the proof. □

3.2. Sliding mode controller design with unknown dynamics

In this section a sliding mode controller with unknown dynamics is derived.

Theorem 3.2. (Sliding mode controller design with unknown dynamics) To suppress the unknown dynamics a sign function can be added to sliding surfaces. By taking sliding surfaces derivatives $\dot{s}_{ki} = -\eta s_{ki} - \varepsilon_{ki} sign(s_{ki})$, $(k = 1, 2, 3, 4)$ where $\varepsilon_{ki} > 0$, $\eta_{ki} > 0$ are positive constants, the controllers can be derived as:

$$\begin{aligned} u_{1i} &= \frac{1}{a_{11}g_{1i}}\left\{a_{11}\left(\ddot{z}_i^d - f_{1i}\right) + a_{12}\left(\dot{z}_i^d - \dot{z}_i\right) + \eta_{1i}s_{1i} + \varepsilon_{1i}\,\mathrm{sign}(s_{1i})\right\} \\ u_{2i} &= \frac{1}{a_{21}g_{2i} + a_{23}g_{3i}}\left\{\begin{array}{l} a_{21}\left(\ddot{x}_i^d - f_{2i}\right) + a_{22}\left(\ddot{x}_i^d - \dot{x}_i\right) + a_{23}\left(\ddot{\phi}_i^d - f_{3i}\right) \\ + a_{24}\left(\dot{\phi}_i^d - \dot{\phi}_i\right) + \eta_{2i}s_{2i} + \varepsilon_{2i}\,\mathrm{sign}(s_{2i})\end{array}\right\} \\ u_{3i} &= \frac{1}{a_{31}g_{4i} + a_{33}g_{5i}}\left\{\begin{array}{l} a_{31}\left(\ddot{y}_i^d - f_{4i}\right) + a_{32}\left(\dot{y}_i^d - \dot{y}_i\right) + a_{33}\left(\ddot{\theta}_i^d - f_{5i}\right) \\ + a_{34}\left(\dot{\theta}_i^d - \dot{\theta}_i\right) + \eta_{3i}s_{3i} + \varepsilon_{3i}\,\mathrm{sign}(s_{3i})\end{array}\right\} \\ u_{4i} &= \frac{1}{a_{41}g_{6i}}\left\{\left(\ddot{\psi}_i^d - f_{6i}\right) + a_{42}\left(\dot{\psi}_i^d - \dot{\psi}_i\right) + \eta_{4i}s_{4i} + \varepsilon_{4i}\,\mathrm{sign}(s_{4i})\right\}. \end{aligned} \tag{19}$$

Applying the controllers to the system with unknown dynamics, all sliding surfaces are asymptotically stable.

P r o o f . Let the Lyapunov function for one quadrotor be as:

$$V_i = \sum_{k=1}^{4} \frac{s_{ki}^2}{2} \tag{20}$$

and by taking the derivative just as it was taken in equation (17) and using controllers equation (19) into equation (20) gives:

$$\begin{aligned} \dot{V}_i &= \sum_{k=1}^{4} s_{ki}\dot{s}_{ki} \\ &= \sum_{k=1}^{4} s_{ki}(a_{11}f_{ki} - \eta_{ki}s_{ki} - \varepsilon_{ki}\,\mathrm{sign}(s_{ki})) \\ &= \sum_{k=1}^{4} s_{ki}a_{11}f_{ki} - \eta_{ki}s_{ki}^2 - \varepsilon_{ki}\,|s_{ki}|. \end{aligned} \tag{21}$$

Hence for any $\varepsilon_{ki} > 0$, $\eta_{ki} > 0$ positive constants derivative of equation (21):

$$\dot{V}_i = \sum_{k=1}^{4} |s_{ki}|\,(a_{11}f_{ki} - \eta_{ki}s_{ki} - \varepsilon_{ki}) \leq 0. \tag{22}$$

If $\varepsilon_{ki} > |a_{11}f_{ki}|$ then the system is asymptotically stable. This concludes the proof. □

3.3. Neuro-sliding mode controller design

For the proposed controller design, quadrotor dynamics with payload that were given in equation (10) are supposed to be unknown and for estimating the unknown dynamics neural network estimation is used. The unknown dynamics f_{ji} $\forall j = 1, 2, 3, 4, 5, 6$ can be given as:

$$f_{ji} = \Theta_{ji}^T \sigma\left(H_{ji}^T \varpi_{ji}\right) + \chi_{ji} \tag{23}$$

where i is number of quadrotors, $\Theta_{ji} \in \mathbb{R}^{2\times h}$ is the bounded desired NN weights that satisfying $\frac{k_n}{2}\|\Theta_{ji}\|^2 \leq \Theta_M$ with $\Theta_M > 0$ a constant, $k_n > 0$ is the NN learning rate and will be defined later, h is the hidden layer neuron number, $\sigma\left(H_{ji}\varpi_{ji}\right)$ is the base function with $H_{ji}^T \in \mathbb{R}^{h\times n}$ is the mapping between the inputs and hidden-layer neurons ,n is the number of inputs to the NN, χ_{ji} is the bounded NN reconstruction error satisfying $\frac{1}{2}\chi_{ji}^2 \leq \chi_M$, with χ_M being a positive constant.

Remark 3.3. Since the uncertain nonlinear dynamics of interconnected system, f_{ji} given in equation (23) will be functions of both the dynamics of the ith UAV and its neighbours, therefore the neural network inputs ϖ_{ji} will consist of the states of both the ith UAV and its neighbours.

The unknown weights could be approximated as $\hat{\Theta}_{ji}$ and approximated uncertain dynamics could be written as:

$$\hat{f}_{ji} = \hat{\Theta}_{ji}^T \sigma \left(H_{ji}^T \varpi_{ji} \right). \tag{24}$$

Estimation error of the NN weight could be written as $\tilde{\Theta}_{ji} = \Theta_{ji} - \hat{\Theta}_{ji}$ and the estimation error dynamics could be defined as $\dot{\tilde{\Theta}}_{ji} = -\dot{\hat{\Theta}}_{ji}$. Then, estimated dynamics can be defined as:

$$\begin{aligned} \tilde{f}_{ji} &= f_{ji} - \hat{f}_{ji} \\ &= \Theta_{ji}^T \sigma \left(H_{ji}^T \varpi_{ji} \right) + \chi_{ji} - \hat{\Theta}_{ji}^T \sigma \left(H_{ji}^T \varpi_{ji} \right) \\ &= \tilde{\Theta}_{ji}^T \sigma \left(H_{ji}^T \varpi_{ji} \right) + \chi_{ji}. \end{aligned} \tag{25}$$

with defined estimated dynamic the controllers in equation (15) can be rearranged as:

$$\begin{aligned} u_{1i} &= \frac{1}{a_{11}} \left\{ a_{11} \left(\ddot{z}_i^d - \hat{f}_{1i} \right) + a_{12} \left(\dot{z}_i^d - \dot{z}_i \right) + \eta_{1i} s_{1i} \right\} \\ u_{2i} &= \frac{1}{a_{21} + a_{23}} \left\{ \begin{array}{l} a_{21} \left(\ddot{x}_i^d - \hat{f}_{2i} \right) + a_{22} \left(\dot{x}_i^d - \dot{x}_i \right) \\ + a_{23} \left(\ddot{\phi}_i^d - \hat{f}_{3i} \right) + a_{24} \left(\dot{\phi}_i^d - \dot{\phi}_i \right) + \eta_{2i} s_{2i} \end{array} \right\} \\ u_{3i} &= \frac{1}{a_{31} + a_{33}} \left\{ \begin{array}{l} a_{31} \left(\ddot{y}_i^d - \hat{f}_{4i} \right) + a_{32} \left(\dot{y}_i^d - \dot{y}_i \right) \\ + a_{33} \left(\ddot{\theta}_i^d - \hat{f}_{5i} \right) + a_{34} \left(\dot{\theta}_i^d - \dot{\theta}_i \right) + \eta_{3i} s_{3i} \end{array} \right\} \\ u_{4i} &= \frac{1}{a_{41}} \left\{ \left(\ddot{\psi}_i^d - \hat{f}_{6i} \right) + a_{42} \left(\dot{\psi}_i^d - \dot{\psi}_i \right) + \eta_{4i} s_{4i} \right\}. \end{aligned} \tag{26}$$

Theorem 3.4. (Neuro-sliding mode controller design) Given the sliding surface dynamics in equation (14) let the controllers be as in equation (25) and let adaptation law for estimated weights be as:

$$\dot{\hat{\Theta}}_{ji} = -k_n \hat{\Theta}_{ji} + s_{ji} a_{ji1} \sigma \left(H_{ji} \varpi_{ji} \right) \forall j = 1, 2, 3, 4. \tag{27}$$

Then, all sliding surface functions and NN weight estimation errors will be SGUUB.

P r o o f . Let the Lyapunov function for sliding surface functions be:

$$V_i = \sum_{j=1}^{4} \left(\frac{1}{2} {s_{ji}}^2 + \frac{1}{2} \left(\tilde{\Theta}_{ji}^T \tilde{\Theta}_{ji} \right) \right). \tag{28}$$

And by taking the derivative of equation (28) :

$$\begin{aligned}
\dot{V}_i &= \sum_{j=1}^{4}\left(s_{ji}\dot{s}_{ji} + \tilde{\Theta}_{ji}^{T}\dot{\tilde{\Theta}}_{ji}\right)\\
&= s_{1i}\dot{s}_{1i} + s_{2i}\dot{s}_{2i} + s_{3i}\dot{s}_{3i} + s_{4i}\dot{s}_{4i}\\
&+ \tilde{\Theta}_{1i}^{T}\dot{\tilde{\Theta}}_{1i} + \tilde{\Theta}_{2i}^{T}\dot{\tilde{\Theta}}_{2i} + \tilde{\Theta}_{3i}^{T}\dot{\tilde{\Theta}}_{3i} + \tilde{\Theta}_{4i}^{T}\dot{\tilde{\Theta}}_{4i}\\
&= s_{1i}\left(a_{11}\left(\ddot{z}_i^{d} - f_{1i} + g_{1i}u_{1i}\right) + a_{12}\left(\dot{z}_i^{d} - \dot{z}_i\right)\right)\\
&+ s_{2i}\begin{pmatrix} a_{21}\left(\ddot{x}_i^{d} - f_{2i} + g_{2i}u_{2i}\right) + a_{22}\left(\dot{x}_i^{d} - \dot{x}_i\right)\\ +a_{23}\left(\ddot{\phi}_i^{d} - f_{3i} + g_{3i}u_{2i}\right) + a_{24}\left(\dot{\phi}_i^{d} - \dot{\phi}_i\right)\end{pmatrix}\\
&+ s_{3i}\begin{pmatrix} a_{31}\left(\ddot{y}_i^{d} - f_{4i} + g_{4i}u_{3i}\right) + a_{32}\left(\dot{x}_i^{d} - \dot{x}_i\right)\\ +a_{33}\left(\ddot{\theta}_i^{d} - f_{5i} + g_{5i}u_{3i}\right) + a_{34}\left(\dot{\theta}_i^{d} - \dot{\theta}_i\right)\end{pmatrix}\\
&+ s_{4i}\left(a_{41}\left(\ddot{\psi}_i^{d} - f_{6i} + g_{6i}u_{4i}\right) + a_{42}\left(\dot{\psi}_i^{d} - \dot{\psi}_i\right)\right)\\
&- \tilde{\Theta}_{1i}^{T}\dot{\tilde{\Theta}}_{1i} - \tilde{\Theta}_{2i}^{T}\dot{\tilde{\Theta}}_{2i} - \tilde{\Theta}_{3i}^{T}\dot{\tilde{\Theta}}_{3i} - \tilde{\Theta}_{4i}^{T}\dot{\tilde{\Theta}}_{4i}
\end{aligned} \tag{29}$$

using the controllers in equation (26) into equation (29) yields:

$$\begin{aligned}
\dot{V}_i &= -\eta_{1i}s_{1i}^{2} - \eta_{2i}s_{2i}^{2} - \eta_{3i}s_{3i}^{2} - \eta_{4i}s_{4i}^{2}\\
&\quad + s_{1i}a_{11}\tilde{f}_{1i} + s_{2i}a_{21}\tilde{f}_{2i} + s_{2i}a_{23}\tilde{f}_{3i} + s_{3i}a_{31}\tilde{f}_{4i} + s_{3i}a_{33}\tilde{f}_{5i} + s_{4i}a_{41}\tilde{f}_{6i}\\
&\quad - \tilde{\Theta}_{1i}^{T}\dot{\hat{\Theta}}_{1i} - \tilde{\Theta}_{2i}^{T}\dot{\hat{\Theta}}_{2i} - \tilde{\Theta}_{3i}^{T}\dot{\hat{\Theta}}_{3i} - \tilde{\Theta}_{4i}^{T}\dot{\hat{\Theta}}_{4i}\\
\dot{V}_i &= -\sum_{j=1}^{4}\eta_{ji}s_{ji}^{2} + \sum_{j=1}^{4}s_{ji}a_{j1}\left(\tilde{\Theta}_{ji}^{T}\sigma\left(H_{ji}^{T}\varpi_{ji}\right) + \chi_{ji}\right) - \sum_{j=1}^{4}\tilde{\Theta}_{ji}^{T}\dot{\hat{\Theta}}_{ji}\\
&= -\sum_{j=1}^{4}\eta_{ji}s_{ji}^{2} + \sum_{j=1}^{4}s_{ji}a_{j1}\left(\tilde{\Theta}_{ji}^{T}\sigma\left(H_{ji}^{T}\varpi_{ji}\right)\right) + \sum_{j=1}^{4}s_{ji}a_{j1}\chi_{ji} - \sum_{j=1}^{4}\tilde{\Theta}_{ji}^{T}\dot{\hat{\Theta}}_{ji}
\end{aligned} \tag{30}$$

by implementing the update laws in equation (27) into equation (30) than we can get:

$$\begin{aligned}
\dot{V}_i &= -\sum_{j=1}^{4}\eta_{ji}s_{ji}^{2} + \sum_{j=1}^{4}s_{ji}a_{j1}\left(\tilde{\Theta}_{ji}^{T}\sigma\left(H_{ji}^{T}\varpi_{ji}\right)\right) + \sum_{j=1}^{4}s_{ji}a_{j1}\chi_{ji}\\
&\quad - \sum_{j=1}^{4}\tilde{\Theta}_{ji}^{T}\left(-k_n\hat{\Theta}_{ji} + s_{ji}a_{j1}\sigma\left(H_{ji}\varpi_{ji}\right)\right)\\
&= -\sum_{j=1}^{4}\eta_{ji}s_{ji}^{2} + \sum_{j=1}^{4}s_{ji}a_{j1}\left(\tilde{\Theta}_{ji}^{T}\sigma\left(H_{ji}^{T}\varpi_{ji}\right)\right) + \sum_{j=1}^{4}s_{ji}a_{j1}\chi_{ji} + k_n\sum_{j=1}^{4}\tilde{\Theta}_{ji}^{T}\hat{\Theta}_{ji}\\
&\quad - \sum_{j=1}^{4}s_{ji}a_{j1}\tilde{\Theta}_{ji}^{T}\left(\sigma\left(H_{ji}\varpi_{ji}\right)\right)
\end{aligned} \tag{31}$$

$$= -\sum_{j=1}^{4} \eta_{ji} s_{ji}^2 + \sum_{j=1}^{4} s_{ji} a_{j1} \chi_{ji} + k_n \sum_{j=1}^{4} \tilde{\Theta}_{ji}^T \left(\Theta_{ji} - \tilde{\Theta}_{ji} \right)$$
$$= -\sum_{j=1}^{4} \eta_{ji} s_{ji}^2 + \sum_{j=1}^{4} s_{ji} a_{j1} \chi_{ji} - k_n \sum_{j=1}^{4} \left\| \tilde{\Theta}_{ji} \right\|^2 + k_n \sum_{j=1}^{4} \tilde{\Theta}_{ji}^T \Theta_{ji} .$$

Lemma 3.5. (Qian and Lin in [35]) The following Young's inequality is true for $a, b \geq 0$ and $p, q > 1$ such that $\frac{1}{p} + \frac{1}{q} = 1$:

$$ab \leq \frac{a^p}{p} + \frac{b^q}{q}. \tag{32}$$

Following inequalities hold from Young's inequality in Lemma 3.5:

$$\begin{aligned} k_n \sum_{j=1}^{4} \tilde{\Theta}_{ji}^T \Theta_{ji} &\leq \frac{k_n}{2} \sum_{j=1}^{4} \left\| \tilde{\Theta}_{ij} \right\|^2 + \frac{k_n}{2} \sum_{j=1}^{4} \| \Theta_{ji} \|^2 \\ \sum_{j=1}^{4} s_{ji} a_{ji1} \chi_{ji} &\leq \frac{1}{2} \sum_{j=1}^{4} s_{ji}^2 a_{ji1} + \frac{1}{2} \sum_{j=1}^{4} a_{ji1} \chi_{ji}^2 \end{aligned} \tag{33}$$

by using equation (33) and the upper bounds of both NN approximation errors and the NN weight estimation errors, respectively equation (31) can be rewritten as:

$$\begin{aligned} \dot{V}_i &= -\sum_{j=1}^{4} \eta_{ji} s_{ji}^2 + \frac{1}{2} \sum_{j=1}^{4} s_{ji}^2 a_{j1} + \frac{1}{2} \sum_{j=1}^{4} a_{j1} \chi_{ji}^2 - k_n \sum_{j=1}^{4} \left\| \tilde{\Theta}_{ji} \right\|^2 \\ &+ \frac{k_n}{2} \sum_{j=1}^{4} \left\| \tilde{\Theta}_{ji} \right\|^2 + \frac{k_n}{2} \sum_{j=1}^{4} \| \Theta_{ji} \|^2 \\ &= -\sum_{j=1}^{4} \left(\eta_{ji} - \frac{a_{j1}}{2} \right) s_{ji}^2 - \frac{k_n}{2} \sum_{j=1}^{4} \left\| \tilde{\Theta}_{ji} \right\|^2 + \chi_M + \Theta_M. \end{aligned} \tag{34}$$

Provided with the controller gain satisfies $\eta_{ji} > \frac{a_{j1}}{2}$ $\forall j = 1, 2, 3, 4$ the stability bounds can be given as;

$$-\sum_{j=1}^{4} \left(\eta_{ji} - \frac{a_{j1}}{2} \right) s_{ji}^2 + \chi_M + \Theta_M < 0 \Rightarrow |s_{ji}| > \sqrt{\frac{\chi_M + \Theta_M}{\left(\eta_{ji} - \frac{a_{j1}}{2} \right)}} \tag{35}$$

$$\text{or } -\frac{k_n}{2} \sum_{j=1}^{4} \left\| \tilde{\Theta}_{ji} \right\|^2 + \chi_M + \Theta_M < 0 \Rightarrow \left\| \tilde{\Theta}_{ji} \right\| > \sqrt{\frac{2 \left(\chi_M + \Theta_M \right)}{k_n}}. \tag{36}$$

Hence, the NN weight estimation errors and sliding surface functions will be SGUUB. This concludes the proof. □

Remark 3.6. Using a neural network component in the control structure technique reduces control input and chattering while optimizing error performance of trajectory tracking.

Next, simulation results are given and evaluated.

4. NUMERICAL SIMULATIONS AND RESULTS

To verify the effectiveness of the proposed controller, an interconnected system consists of three quadrotor UAVs that transport a suspended payload was modeled and simulations were carried out in MATLAB. As a solver, ode45 was used, and simulation time for all simulations was 120 seconds. For this purpose, three simulations were carried out. First, an SMC was applied to the system under the assumption that all dynamics were known. In a second simulation, an SMC with unknown dynamics was applied to the system. In the last simulation, a neuro-sliding mode controller was applied to the system.

The parameters of each quadrotor are chosen as:

$$m = 1.1kg, m_L = 0.5kg, g = 9.8m/s^2, J_r = \ 0.2Ns^2/rad, L = 4m, l = 0.21m,$$
$$I_x = I_y = 1.22Ns^2/rad, I_z = 2.22Ns^2/rad, K_1 = K_2 = K_3 = 0.1Ns/rad,$$
$$b = 5Ns^2, K_4 = K_5 = K_6 = 0.12Ns/rad, d = 2N/ms^2.$$

Initial conditions selected as:

$$\mathrm{X}_1(0)= 0, \quad \mathrm{X}_2(0) = \text{-}3, \quad \mathrm{X}_3(0) = 2, Y_1(0) = 5, \quad Y_2(0) = 3.5, \quad Y_3(0) = 2,$$
$$Z_1(0) = 0, \quad Z_2(0) = 0, \quad Z_3(0) = 0, \phi_i(0) = 0, \quad \theta_i(0) = 0, \quad \Psi_i(0) = 0, \text{ i=1,2,3.}$$

$a_{21}, a_{22}, a_{23}, a_{24}, a_{31}, a_{32}, a_{33}, a_{34}$ controller gains were obtained in detail and they can be found in our previous work [2] and the rest of the gains are selected as:

$$a_{11} = 2, \ a_{12} = 2, \ \ a_{41} = 2, \ a_{42} = 2, a_{13} = a_{14} = a_{43} = a_{44} = 0.$$

For quadrotors the desired trajectories are chosen as:

$$\mathrm{X}_{1d}= \mathrm{t}, \mathrm{X}_{2d}= \text{t-}\sqrt{3}, \mathrm{X}_{3d} = \text{t+}\sqrt{3}, Y_{1d} = \mathrm{t}, Y_{2d}= \text{t-3}, Y_{3d} = \text{t-3},$$
$$Z_{1d}(0) = \mathrm{K}, Z_{2d}(0) = \mathrm{K}, Z_{3d}(0) = \mathrm{K}, \ \mathrm{K} = 8 \ m, \phi_{id} = 0, \theta_{id} = 0, \Psi_{id} = 0.5, \text{ i=1,2,3.}$$

The desired angles for payload are selected as:

$$\alpha_1^d = \alpha_L^d = \pi/6, \beta_1^d = \beta_L^d = \pi/2, \beta_2^d = \frac{7\pi}{6}, \beta_3^d = \frac{11\pi}{6}.$$

During the simulations, the initial values of neural network weights are set to zero and the neurons of hidden layer are randomly selected.

Assumption 4.1. The simulations included a standard SMC structure for comparison. A saturation function defined as follows is used in instead of the sign function in the SMC structure to lessen the chattering effect and, consequently, the computational burden.

$$sat(x) = \begin{cases} x/\kappa, & |x| \leq \kappa \\ sign(x), & |x| > \kappa \end{cases} \tag{37}$$

where $\kappa > 0$, and it was taken to be $\kappa = 0.5$ in the simulations.

Remark 4.2. It is worth noting that the above assumption was only used for classical SMC in order to perform a faster simulation, not for the proposed controller.

First simulation was carried out for SMC with the presumption that all dynamics of the system are known. Position errors of quadrotors are given in Figures 7, 8 and 9.

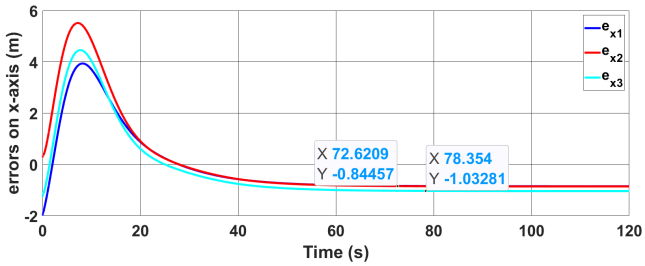

Fig. 7. x position errors of UAVs for SMC with known dynamics.

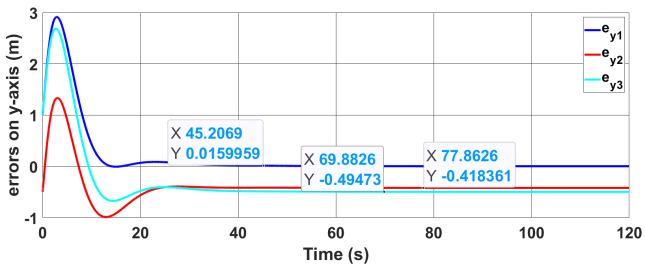

Fig. 8. y position errors of UAVs for SMC with known dynamics.

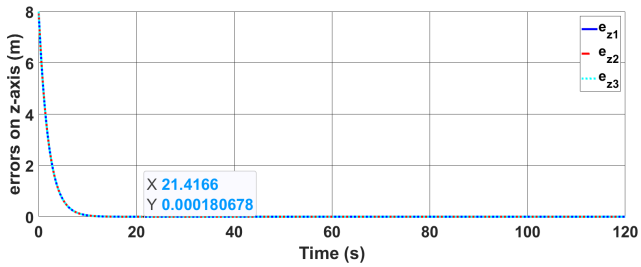

Fig. 9. z position errors of UAVs for SMC with known dynamics.

Even assuming that the dynamics are known, it is seen that the classical SMC cannot prevent noticeable errors in position tracking. For x positions errors occur between

0.84m to 1m for quadrotors. Looking at the y position errors, it is seen that the second and third quadrotors have tracking errors of around 0.5 m, although the error of the first quadrotor is close to zero. On z axes, quadrotors settle to desired values. In the beginning, the system required very high u_{1i} controller input values of about 250 N, as can be observed in Figure 10. After around 10 seconds, the input value has stabilized at around 16 N. Despite having small values, controller inputs u_{2i} and u_{3i} demonstrate high chattering as it is accepted from classical SMC shown in Figures 11 and 12, and u_{4i} controller input values are around 55 N as shown in Figure 13. As it can be understood from these figures, classical SMC needs very high input signal values, especially at the beginning, and a chattering effect is inevitable in control signals.

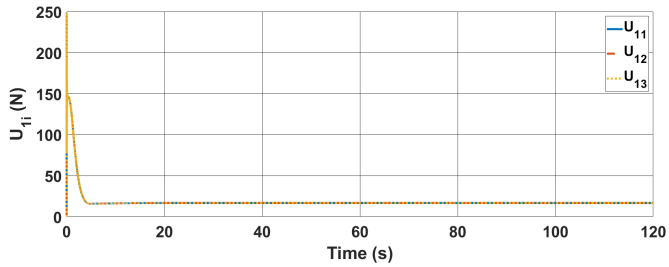

Fig. 10. u_{1i} control inputs for SMC with known dynamics.

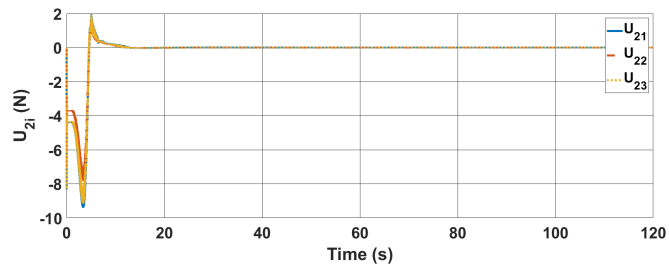

Fig. 11. u_{2i} control inputs for SMC with known dynamics.

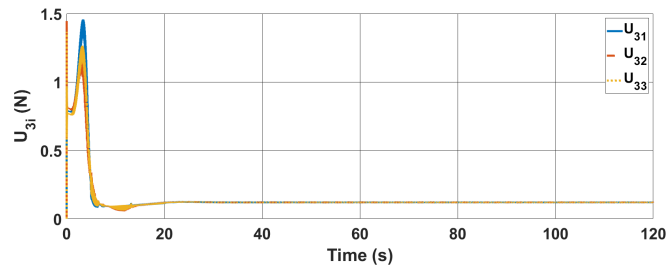

Fig. 12. u_{3i} control inputs for SMC with known dynamics.

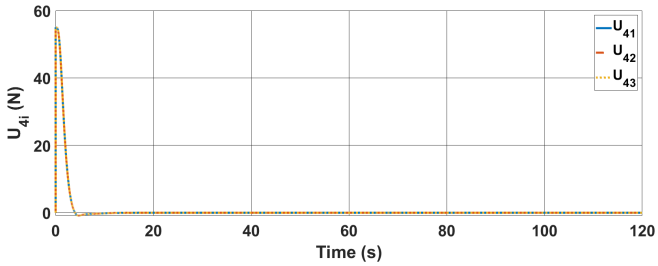

Fig. 13. u_{4i} control inputs for SMC with known dynamics.

A second simulation was carried out for an SMC with unknown dynamics. In this case, controllers have been designed by taking into account the unknown dynamics that will be encountered in real applications. Figures 14, 15 and 16 show quadrotor position errors in the x, y, and z axes. When the errors along the x-axis are analyzed, it is discovered that the second and third quadrotors have significant errors of around 0.86 m, whilst the first quadrotor follows the reference with an acceptable error of approximately 0.1 m. Similarly, in the y-axis, the first quadrotor can follow the reference with a small error, while the second and third quadrotors can follow the reference with an error of around 0.4 m. In addition, in order for the quadrotors to settle into the reference trajectories in the x and y axes because of the effect of unknown dynamics, it takes a significant amount of extra time when compared to the prior simulation.A deviation of around 0.6 meters occurs in the z-axis for each of the three quadrotors. The changes in control signals are given in Figures 17, 18 and 19. It is seen that the chattering effects seriously distort the control signals due to the unknown dynamics. u_{1i} controller input values decreased to around 50 N from 250 N compared to the first simulation. But as it can be observed from the figure, a very high chattering is generated in control signals. As in u_{1i}, despite the fact that the inputs u_{2i} and u_{3i} are small, undesirable high sparks are observed in the control inputs. u_{4i} controller input values are around 110 N, as given in Figure 20. It is also clear that the u_{4i} controller input values have doubled in this simulation. These simulation results clearly show how unknown dynamics can create negative effects in the controlled system. In order to eliminate these negativities as much as possible, the final simulation will show the contribution of the proposed controller in this study.

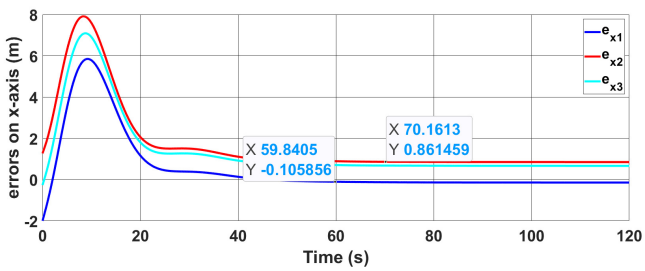

Fig. 14. x position errors of UAVs for SMC with unknown dynamics.

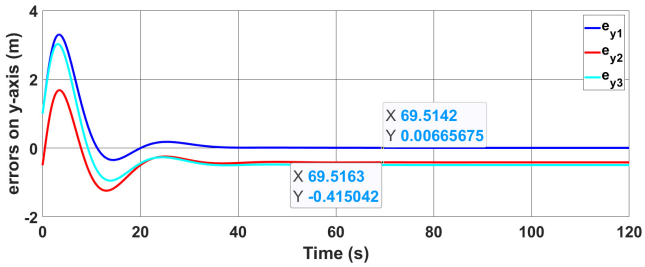

Fig. 15. y position errors of UAVs for SMC with unknown dynamics.

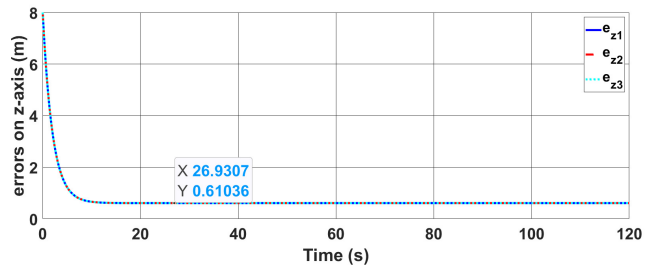

Fig. 16. z position errors of UAVs for SMC with unknown dynamics.

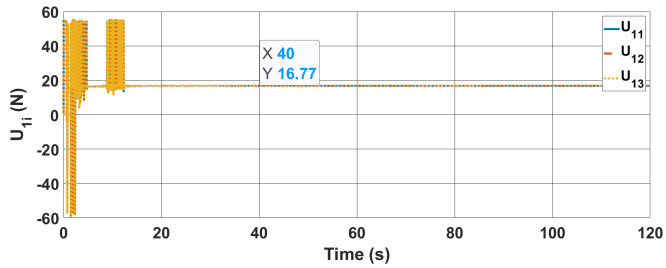

Fig. 17. u_{1i} control inputs for SMC with unknown dynamics.

In the third simulation, neuro-SMC, the controller proposed in the study, was applied to the system. The changes in the position errors of the quadrotors in the three axes is given in Figures 21, 22 and 23. As can be clearly observed from the figures, the errors in the reference tracking of the three quadrotors in the x, y and y axes reach the neighborhood of zero asymptotically with the proposed controller.

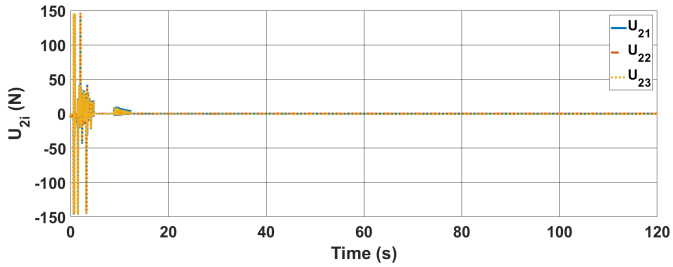

Fig. 18. u_{2i} control inputs for SMC with unknown dynamics.

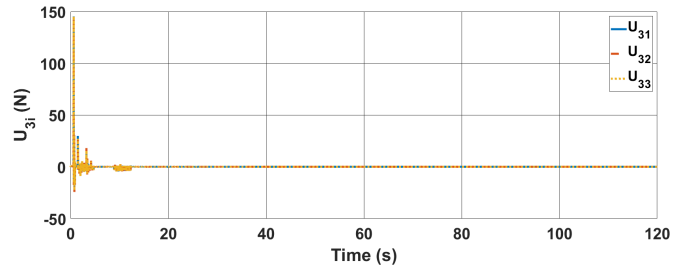

Fig. 19. u_{3i} control inputs for SMC with unknown dynamics.

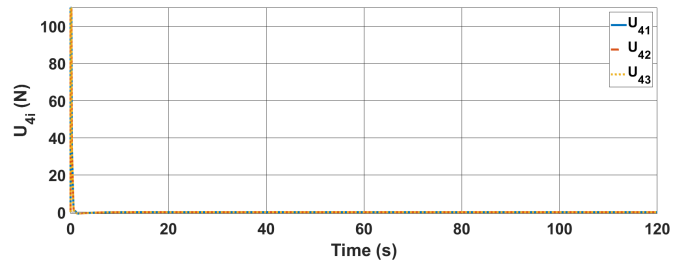

Fig. 20. u_{4i} control inputs for SMC with unknown dynamics.

Variations in errors of quadrotor angles are given in Figures 24, 25 and 26. It can be observed from the figures that the variations in the angles are also very small.

Control inputs for the proposed controller are given in Figures 27, 28 and 29. It is clear that the high chattering effects that were brought on by unknown dynamics in the earlier simulation are swiftly eradicated owing to the neural network component that is included in the suggested controller. Until the neural network learns the system dynamics, it is seen that a certain amount of unwanted sparks can occur in the control signals. However, when the dynamics are learned, it is seen that the control signals quickly settle to nominal values. It is also seen that the amplitudes of sparks in the control signals are significantly reduced compared to the chattering effect. u_{1i} controller

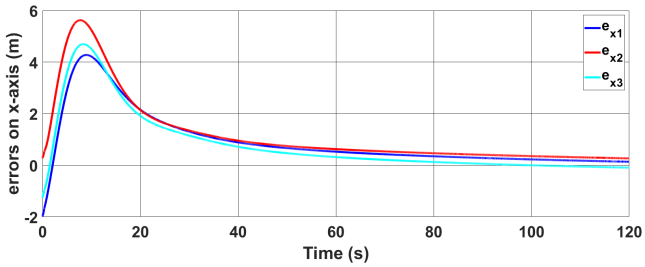

Fig. 21. x position errors of UAVs for neuro-SMC with unknown dynamics.

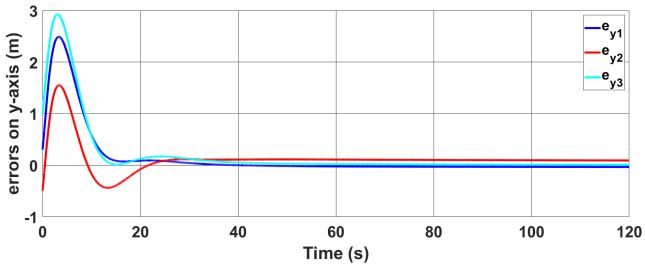

Fig. 22. y position errors of UAVs for neuro-SMC with unknown dynamics.

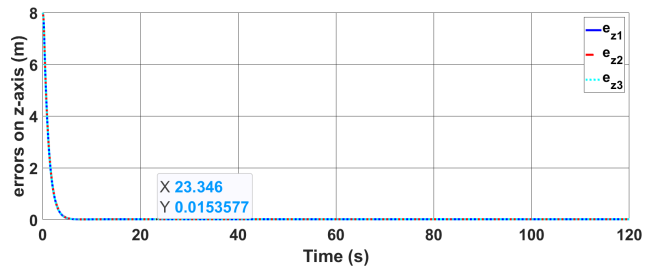

Fig. 23. z position errors of UAVs for neuro-SMC with unknown dynamic.

input values are less than 40N in the beginning. As it can be observed from the figure chattering is reduced significantly. As in u_{1i} , inputs u_{2i} and u_{3i} are also small and chattering effects decreased. u_{4i} controller input values are around 40 N as shown in Figure 30. The chattering continues until the neural network learns the unknown dynamics. After the learning process is completed, the chattering in the control signals disappears. This clearly shows how the proposed controller successfully counteracts the chattering effect of classical SMC with known and unknown dynamics as presented in the first two simulations.

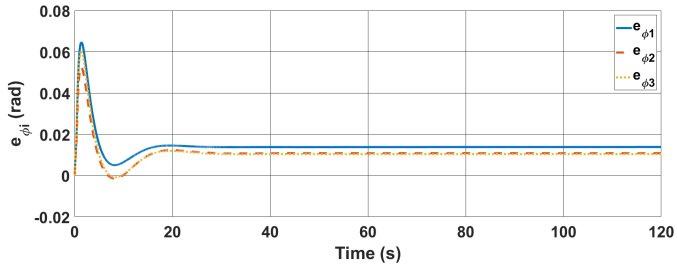

Fig. 24. Errors of roll angles of UAVs for neuro-SMC with unknown dynamics.

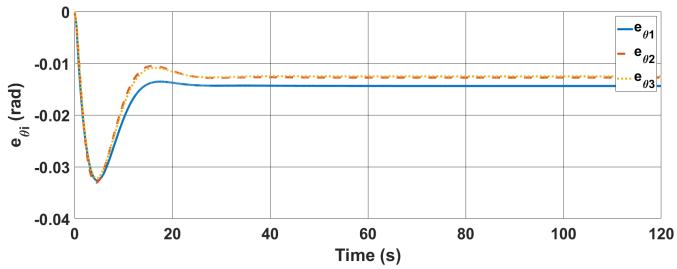

Fig. 25. Errors of pitch angles of UAVs for neuro-SMC with unknown dynamics.

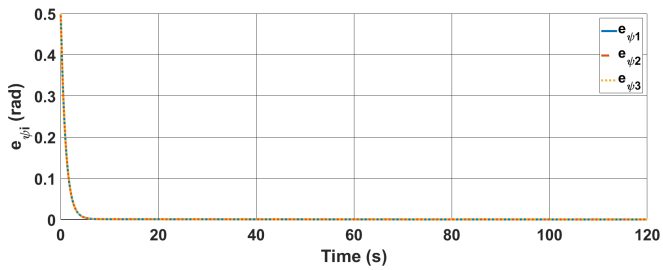

Fig. 26. Errors of yaw angles of UAVs for neuro-SMC with unknown dynamics.

In Figure 31 quadrotors trajectories are plotted in three dimensions. In Figure 32, the convergence rates for neural network neurons are seen. As shown in the figure, they are successfully converging to a non-zero value. While the sliding mode controller provide robustness during the neural network estimation period, neural network based adaptive scheme provides better steady state response. Therefore, neural network rates will change until quadrotors reach steady state and after that point, they converge to a small value showing that estimation is completed.

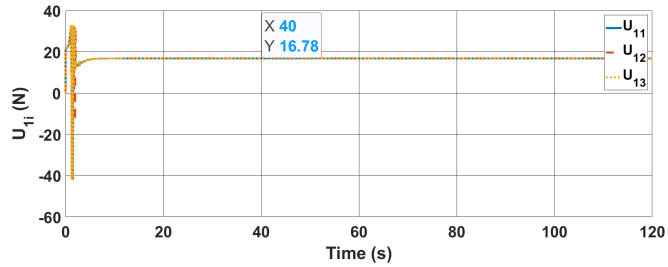

Fig. 27. u_{1i} control inputs for neuro-SMC with unknown dynamics.

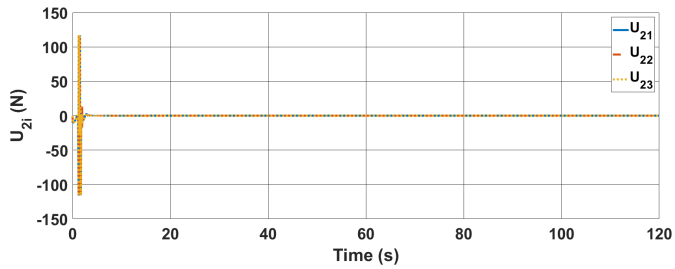

Fig. 28. u_{2i} control inputs for neuro-SMC with unknown dynamics.

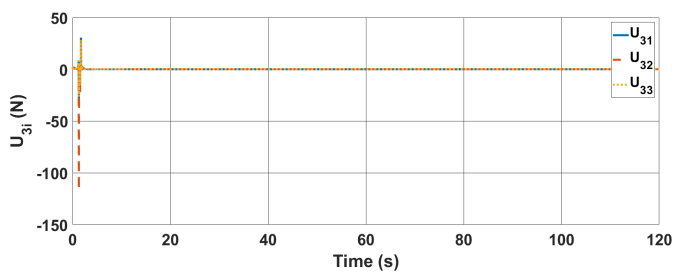

Fig. 29. u_{3i} control inputs for neuro-SMC with unknown dynamics.

5. CONCLUSION

A neuro-sliding mode controller was proposed to control an interconnected quadrotor UAV's system transporting a suspended payload. After obtaining the mathematical model of the load-carrying system with three quadrotors, it was generalized and brought to the form to be used for n-quadrotors. Three different simulations were carried out to display the effectiveness of the proposed controller. First, the system was controlled with an SMC with the assumption that all the system dynamics were known. In this

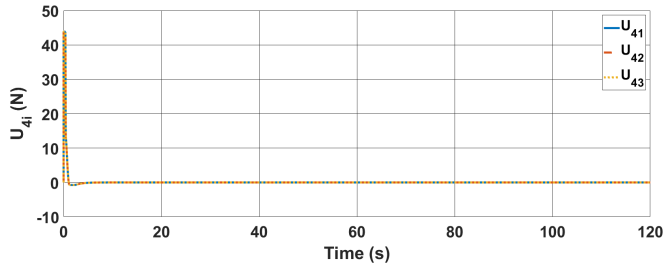

Fig. 30. u_{4i} control inputs for neuro-SMC with unknown dynamics.

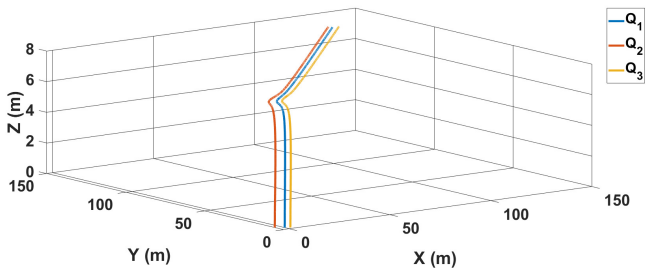

Fig. 31. 3D trajectories of UAVs for neuro-SMC with unknown dynamics.

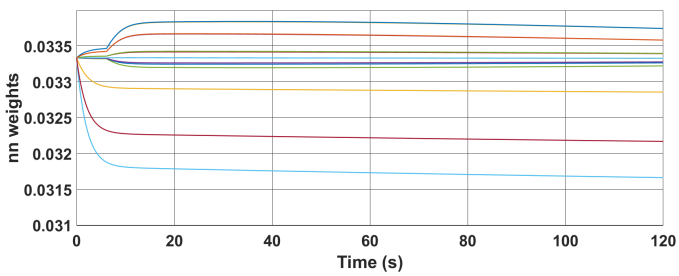

Fig. 32. Convergence rates of neural network weights.

case, although no chattering effect was observed in the control signals, the values of the control signals were found to be very large. In addition, errors were observed in the positional trajectories. Secondly, an SMC was designed with unknown dynamics. In this simulation, as well as errors in trajectory tracking in all three axes due to the effects of unknown dynamics, serious chattering effects were observed in the control signals. In the third and final simulation, the proposed controller neuro-SMC was applied to the system. As it can be observed from the results, while the quadrotors follow the

desired trajectories with high accuracy, a significant improvement has been achieved in the control signals.

Future work includes investigating different sliding surface functions to get a better the robustness of the sliding mode controller part in the proposed controller and applying various artificial intelligence algorithms that can be alternatives to the neural network structure. In addition, formation measurement may be an intriguing area for future research since it might be imprecise and noisy, making it challenging for neural network components to learn the unknown dynamics.

(Received November 24, 2022)

REFERENCES

[1] E. Altug, J. P. Ostrowski, and C. J. Taylor: Control of a quadrotor helicopter using dual camera visual feedback. Int. J. Rob. Res. *24* (2005), 5, 329–341. DOI:10.1016/j.csm.2005.01.002

[2] Ö. Bingöl and H. M. Güzey: Neuro sliding mode control of quadrotor UAVs carrying suspended payload. Adv. Robot. *35* (2021), 3–4, 255–266. DOI:10.1080/01691864.2020.1870557

[3] Ö. Bingöl and H.-M. Güzey: Finite-time neuro-sliding-mode controller design for quadrotor uavs carrying suspended payload. Drones *6* (2022), 10, 311. DOI:10.3390/drones6100311

[4] Ö. Bingöl and H. M. Güzey: Fixed-time neuro-sliding mode controller design for quadrotor uav transporting a suspended payload. European J. Control *73* (2023), 100879. DOI:10.1016/j.ejcon.2023.100879

[5] M. Bisgaard, A. la Cour-Harbo, and J. Dimon Bendtsen: Adaptive control system for autonomous helicopter slung load operations. Control Eng. Pract., 2010.

[6] S. Bouabdallah, P. Murrieri, and R. Siegwart: Design and control of an indoor micro quadrotor. In: Proc. IEEE International Conference on Robotics and Automation, ICRA'04, IEEE 2004. Vol. 5, pp. 4393–4398. DOI:10.1109/robot.2004.1302409

[7] Y. Chen and H. Chen: Prescribed performance control of underactuated surface vessels' trajectory using a neural network and integral time-delay sliding mode. Kybernetika *59* (2023), 2, 273–293. DOI:10.14736/kyb-2023-2-0273

[8] P. J. Cruz, M. Oishi, and R. Fierro: Lift of a cable-suspended load by a quadrotor: A hybrid system approach. In: Proc. Am. Control Conf. 2015, pp. 1887–1892. DOI:10.1109/acc.2015.7171008

[9] K. K. Dhiman, M. Kothari, and A. Abhishek: Autonomous load control and transportation using multiple quadrotors. J. Aerosp. Inf. Syst. *17* (2020), 8, 417–435. DOI:10.2514/1.i010787

[10] T. Dierks and S. Jagannathan: Output feedback control of a quadrotor UAV using neural networks. IEEE Trans. Neural Networks 2010.

[11] M. Ertugrul and O. Kaynak: Neuro sliding mode control of robotic manipulators. Mechatronics *10* (2000), 1–2, 239–263. DOI:10.1016/S0957-4158(99)00057-4

[12] A. Faust, I. Palunko, P. Cruz, R. Fierro, and L. Tapia: Automated aerial suspended cargo delivery through reinforcement learning. Artif. Intell. 2017.

[13] S. Frikha, M. Djemel, and N. Derbel: A new adaptive neuro-sliding mode control for gantry crane. Int. J. Control Autom. Syst. *16* (2018), 2, 559–565. DOI:10.1007/s12555-017-0070-x

[14] M. Gassner, T. Cieslewski, and D. Scaramuzza: Dynamic collaboration without communication: Vision-based cable-suspended load transport with two quadrotors. In: Proc. IEEE Int. Conf. Robot. Autom. 2017, pp. 5196–5202.

[15] J. Geng and J. W. Langelaan: Cooperative transport of a slung load using load-leading control. J. Guid. Control. Dyn. *43* (2020), 7, 1313–1331. DOI:10.2514/1.G004680

[16] S. Grzonka, G. Grisetti, and W. Burgard: A fully autonomous indoor quadrotor. IEEE Trans. Robot. *28* (2012), 1, 90–100. DOI:10.1109/tro.2011.2162999

[17] K. Guo, J. Jia, X. Yu, L. Guo, and L. Xie: Multiple observers based anti-disturbance control for a quadrotor UAV against payload and wind disturbances. Control Eng. Pract. *102* (2019), 104560. DOI:10.1016/j.conengprac.2020.104560

[18] G. Hoffmann, H. Huang, S. Waslander, and C. Tomlin: Quadrotor helicopter flight dynamics and control: Theory and experiment. In: AIAA Quidance, Navigation and Control Conference and Exhibit 2007, p. 6461.

[19] Z. Hou, P. Lu, and Z. Tu: Nonsingular terminal sliding mode control for a quadrotor UAV with a total rotor failure. Aerosp. Sci. Technol. *98* (2020), 105716. DOI:10.1016/j.ast.2020.105716

[20] J. Hwangbo, I. Sa, R. Siegwart, and M. Hutter: Control of a quadrotor with reinforcement learning. IEEE Robot. Autom. Lett. *2* (2017), 4, 2096–2103. DOI:10.1109/LRA.2017.2720851

[21] Q. Jiang and V. Kumar: The inverse kinematics of cooperative transport with multiple aerial robots. IEEE Trans. Robot. *29* (2013), 1, 136–145. DOI:10.1109/TRO.2012.2218991

[22] J. J. Slotine and S. S. Sastry: Tracking control of nonlinear systems using sliding surfaces. Int. J. Control *38* (1083), 2, 465–492.

[23] T. Lee, M. Leok, and N. B. Mcclamroch: Nonlinear robust tracking control of a quadrotor UAV on SE(3). Asian J. Control *15* (2013), 2, 391–408. DOI:10.1002/asjc.567

[24] R. Lei and L. Chen: Observer-based adaptive sliding mode fault-tolerant control for the underactuated space robot with joint actuator gain faults. Kybernetika *57* (2021), 1, 160–173. DOI:10.14736/kyb-2021-1-0160

[25] Arie Levant: Principles of 2-sliding mode design. Automatica *43* (2007), 4, 576–586. DOI:10.1016/j.automatica.2006.10.008

[26] F. L. Lewis: Neural network control of robot manipulators. IEEE Expert. Syst. their Appl. 1996.

[27] G. Li, R. Ge, and G. Loianno: Cooperative transportation of cable suspended payloads with MAVs using monocular vision and inertial sensing. IEEE Robot. Autom. Lett. *6* (2021), 3, 5316–5323. DOI:10.1109/LRA.2021.3065286

[28] H. Lim, J. Park, D. Lee, and H. J. Kim: Build your own quadrotor: Open-source projects on unmanned aerial vehicles. 2012.

[29] Z. Liu, X. Liu, J. Chen, and Ch. Fang: Altitude control for variable load quadrotor via learning rate based robust sliding mode controller. IEEE Access *7* (2019), 9736–9744. DOI:10.1109/ACCESS.2018.2890450

[30] A. Noordin, M. A. M. Basri, Z.Mohamed, and I. Mat Lazim: Adaptive PID controller using sliding mode control approaches for quadrotor UAV attitude and position stabilization. Arab. J. Sci. Engrg. *46* (2021), 2, 963–981. DOI:10.1007/s13369-020-04742-w

[31] I. Palunko, R. Fierro, and P. Cruz: Trajectory generation for swing-free maneuvers of a quadrotor with suspended payload: A dynamic programming approach. In: Proc. IEEE Int. Conf. Robot. Autom.,2012, pp. 2691–2697. DOI:10.1109/icra.2012.6225213

[32] I. Henrique Beloti Pizetta, A. S. Brandao, and M. Sarcinelli-Filho: Modelling and control of a PVTOL quadrotor carrying a suspended load. In: Int. Conf. Unmanned Aircr. Syst. ICUAS 2015.

[33] F. Plestan, A. Glumineau, and S. Laghrouche: A new algorithm for high-order sliding mode control. Int. J. Robust Nonlinear Control *18* (2008), 4–5, 441–453. DOI:10.1002/rnc.1234

[34] P. Pounds, R. Mahony, and P. Corke: Modelling and control of a large quadrotor robot. Control Eng. Pract. *18* (2010), 7, 691–699. DOI:10.1016/j.conengprac.2010.02.008

[35] Ch. Qian and W. Lin: Non-Lipschitz continuous stabilizers for nonlinear systems with uncontrollable unstable linearization. Syst. Control Lett. *42* (2001), 3, 185–200. DOI:10.1016/S0167-6911(00)00089-X

[36] F. Rossomando, C. Rosales, J. Gimenez, L. Salinas, C. Soria, M. Sarcinelli-Filho, and R. Carelli: Aerial load transportation with multiple quadrotors based on a kinematic controller and a neural SMC DYNAMIC COMPEnsation. J. Intell. Robot. Syst. Theory Appl. *100* (2020), 2, 519–530. DOI:10.1007/s10846-020-01195-z

[37] B. Shirani, M. Najafi, and I. Izadi: Cooperative load transportation using multiple UAVs. Aerosp. Sci. Technol. *84* (2019), 158–169. DOI:10.1016/j.ast.2018.10.027

[38] K. Sreenath, T. Lee, and V. Kumar: Geometric control and differential flatness of a quadrotor UAV with a cable-suspended load. In: 52nd IEEE Conf. Decis. Control, Vol. 2019, pp. 2269–2274.

[39] V. I. Utkin: Survey Paper: Variable structure systems with sliding modes. IEEE Trans. Automat. Control 1977.

[40] M. Vahdanipour and M. Khodabandeh: Adaptive fractional order sliding mode control for a quadrotor with a varying load. Aerosp. Sci. Technol. *86* (2019), 737–747. DOI:10.1016/j.ast.2019.01.053

[41] D. K. D. Villa, A. S. Brandão, and M. Sarcinelli-Filho: A survey on load transportation using multirotor UAVs. J. Intell. Robot. Syst. Theory Appl. *98* (2020), 2, 267–296. DOI:10.1007/s10846-019-01088-w

[42] J. Wang, F. Wang, X. Wang, and L. Yu: Disturbance observer based integral terminal sliding mode control for permanent magnet synchronous motor system. Kybernetika *55* (2019), 3, 586–603. DOI:10.14736/kyb-2019-3-0586

[43] J. J. Xiong and G. Zhang: Sliding mode control for a quadrotor UAV with parameter uncertainties. In: Proc. 2nd Int. Conf. Control. Autom. Robot. ICCAR 2016.

[44] K. Yi, F. Gu, L. Yang, Y. He, and J. Han: Sliding mode control for a quadrotor slung load system. In: Chinese Control Conf. CCC, 2017.

[45] W. You, F. Li, L. Liao, and M. Huang: Data fusion of UWB and IMU based on unscented Kalman filter for indoor localization of quadrotor UAV. IEEE Access *8* (2020), 64971–64981. DOI:10.1109/ACCESS.2020.2985053

[46] G. Yu, D. Cabecinhas, R. Cunha, and C. Silvestre: Nonlinear backstepping control of a quadrotor-slung load system. IEEE/ASME Trans. Mechatronics *24* (2019), 5, 2304–2315. DOI:10.1109/TMECH.2019.2930211

[47] Ch. Zhang, S. Li, and S. Ding: Finite-time output feedback stabilization and control for a quadrotor mini-aircraft. Kybernetika *48* (2012), 2, 206–222.

[48] B. Zhou, J. Pan, F. Gao, and S. Shen: RAPTOR: Robust and perception-aware trajectory replanning for quadrotor fast flight. IEEE Trans. Robot. *37* (2021), 6, 1992–2009. DOI:10.1109/TRO.2021.3071527

[49] X. Zhou, R. Liu, J. Zhang, and X. Zhang: Stabilization of a quadrotor with uncertain suspended load using sliding mode control. In: Proc. ASME Des. Eng. Tech. Conf. 2016. DOI:10.1115/detc2016-60060

Özhan Bingöl, Department of Electrical and Electronics Engineering, Gümüshane, 29000. Turkey.
e-mail: ozhan.bingol@gumushane.edu.tr

Haci Mehmet Güzey, Department of Electrical and Electronics Engineering, Sivas, 58000. Turkey.
e-mail: mehmet.guzey@sivas.edu.tr